Supplemental Figures and Material: Mammalian SEPT9 isoforms direct microtubule-dependent arrangements of septin core heteromers

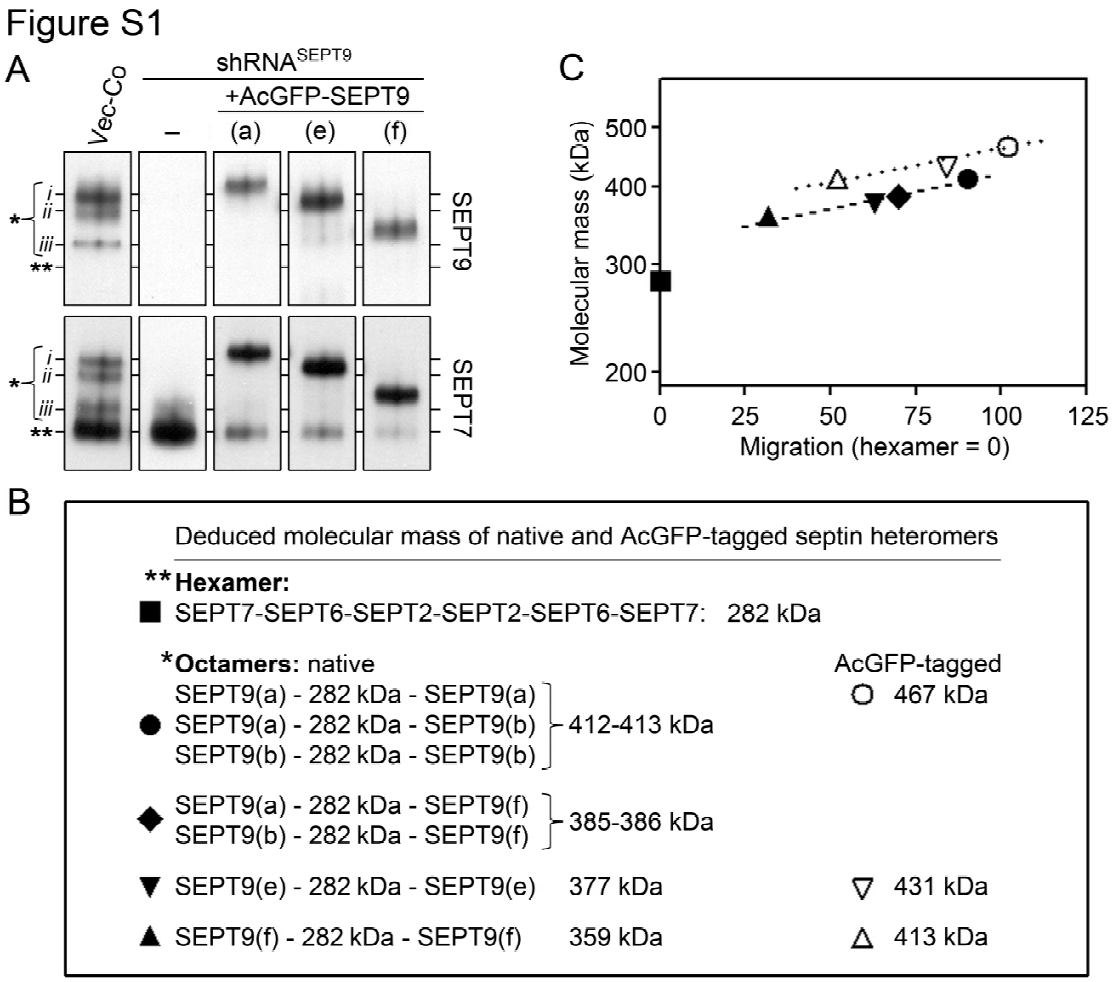

FIGURE S1: Analysis of septin heteromers in cells with endogenous SEPT9 replaced by AcGFP-SEPT9 derivatives

(A) The septin heteromer pools of the transfected K562 cell lines (as described under Figure 4 and 5) were resolved by Blue Native PAGE followed by immuno-detection of SEPT9 (upper panels) and SEPT7 (lower panels). The positions of hexameric (**) and octameric (*) heteromers are indicated. Septin heteromers corresponding to endogenous octamers are denoted *i*, *ii*, and *iii*.

(B) The deduced molecular masses of the indicated native or AcGFP-tagged octamers were calculated with the assumption that all octamers are comprised of the SEPT2, SEPT6, and SEPT7-containing hexamer capped with a SEPT9 protein at each end. Note that while K562 cells also express other members of the SEPT2- and SEPT6 subgroups (see Figure 3A), which can serve as alternative components of the hexamer (Sellin *et al.*, 2011b), their molecular mass are similar to the founding member of each subgroup. Calculations were based on the following molecular masses; SEPT9(a), 65 401 Da; SEPT9(b), 64 681 Da; SEPT9(e), 47 501 Da; SEPT9(f), 38 518 Da; SEPT2, 41 487 Da; SEPT6 (isoform A), 48 872 Da; SEPT7(isoform 1), 50 679 kDa; AcGFP, 26 900 Da.

(C) The correlation between molecular masses and the mobility of native (closed symbols) and AcGFP-tagged (open symbols) heteromers by Blue Native PAGE. Migration of the hexamer is set as 0; symbols indicate the corresponding heteromers as shown in panel (B). Note that the assignment of the endogenous complex *ii* as the 385-386 kDa octamers as in panel B is tentative.

Interpretations:

Recall that K562 cells express three SEPT9 isoforms – two large (a and b that only differ by 0.72 kDa) and one small (isoform f) – each of which can be predicted to cap the septin core hexamer at either end to form an octamer (Figure 4). Analysis of the septin heteromer pool of cell lines in which the three endogenous SEPT9 isoforms are replaced by a single native isoform (Results, Figure 4C, Blue native PAGE) demonstrates that SEPT9 expression directs the octamer to hexamer heteromer ratio. Figure S1A shows the cognate experiment using AcGFP-tagged isoforms (described in Results, Figure 5), which demonstrates that AcGFP-SEPT9 derivative likewise generates the expected increase in the octamer to hexamer ratio.

When native SEPT9 isoforms are expressed (Figure 4C), the octamers generated upon expression of the SEPT9(a) or the SEPT9(f) isoforms have the same mobility as the endogenous octamer complex *i* and *iii*, respectively, which implies that complex *i* can be expected to correspond to octamers capped with either of the large SEPT9 isoforms (a or b), and complex *iii* to octamers capped with isoforms f at both ends. The intermediary sized complex *ii* was thus tentatively assigned as octamers with isoform f at one end and a or b at the other. The corresponding analysis of AcGFP-tagged octamers (Figure S1A) shows that each of the expressed AcGFP-SEPT9 isoform generates uniformly sized octamers. In the case of AcGFP-SEPT9(a) and AcGFP-SEPT9(f), the presence of the AcGFP is identifiable by a shift in mobility as compared to complex *i* and *iii*, respectively.

The molecular mass is considered as the main determinant for separation by Blue Native PAGE, but the shape of protein complexes (i.e. Stoke radius) is also of significance (Wittig *et al.*, 2006). Septin heteromers are rod-shaped and their Stroke radius – as determined by gel filtration (Sellin *et al.*, 2011b) – are notably large relative to the mass. Based on a comparison with commonly used markers (ferritin, Stoke radius 6.10 nm/450 kDa; thyroglobulin, Stoke radius 8.5 nm/670 kDa), Blue Native PAGE analysis predicts a hexamer mass of ~500 kDa, which is a deviation that can be attributed to the elongated shape of the 282 kDa hexamers.

The structure of the variable N-terminal extension of SEPT9 isoforms is unknown and the impact on octamer shape cannot be predicted. Figure S1C shows a plot of molecular masses (listed in Figure S1B) *versus* the mobility of the hexameric heteromer and octamers capped by different SEPT9 isoform derivatives upon separation by Blue native PAGE (Figure S1C). It is evident from these data that, although the predicted masses and mobility of the native and AcGFP tagged octamers show a log-linear relationship (see dashed and dotted lines Figure S1C), the N-terminal extensions affect octamer mobility much more than could be excepted by their increase in mass. For example, the difference in mass between SEPT9(a) and SEPT9(f) is approximately the same as an AcGFP-fusion partner (27 kDa), i.e. the mass of octamers capped with either SEPT9(a) (●) or AcGFP-SEPT9(f) (Δ) is the same (~413 kDa), but the presence of AcGFP affects the mobility much less than the N-terminal extension of SEPT9(a). Relative to the G-domain, SEPT9 isoform a, e, and f have approximately a 295, 131 and 44 residues N-terminal region, respectively, and it is notable that even the N-terminal extension of the SEPT9(e) isoform has a pronounced effect on the mobility of the cognate octamers. Hence, this comparison of native and AcGFP-tagged octamers demonstrates that the N-terminal extension of SEPT9 has properties that facilitate separation of distinct subsets of octameric septin heteromers by the Blue Native PAGE technique.

As outlined above, absolute molecular mass estimates based on the Blue Native PAGE technique can be misleading. Nevertheless, the log-linear mobility correlation of octamers capped with native SEPT9 isoform a, e, and f suggests a correlation with mass among the SEPT9 isoforms. The assignment of complex *ii* as a putative 385-386 kDa complexes composed of the hexamer capped with isoform f at one end and a or b at the other (◆, Figure S1B) is further supported by its mobility correlation shown in Figure S1C.

Figure S2

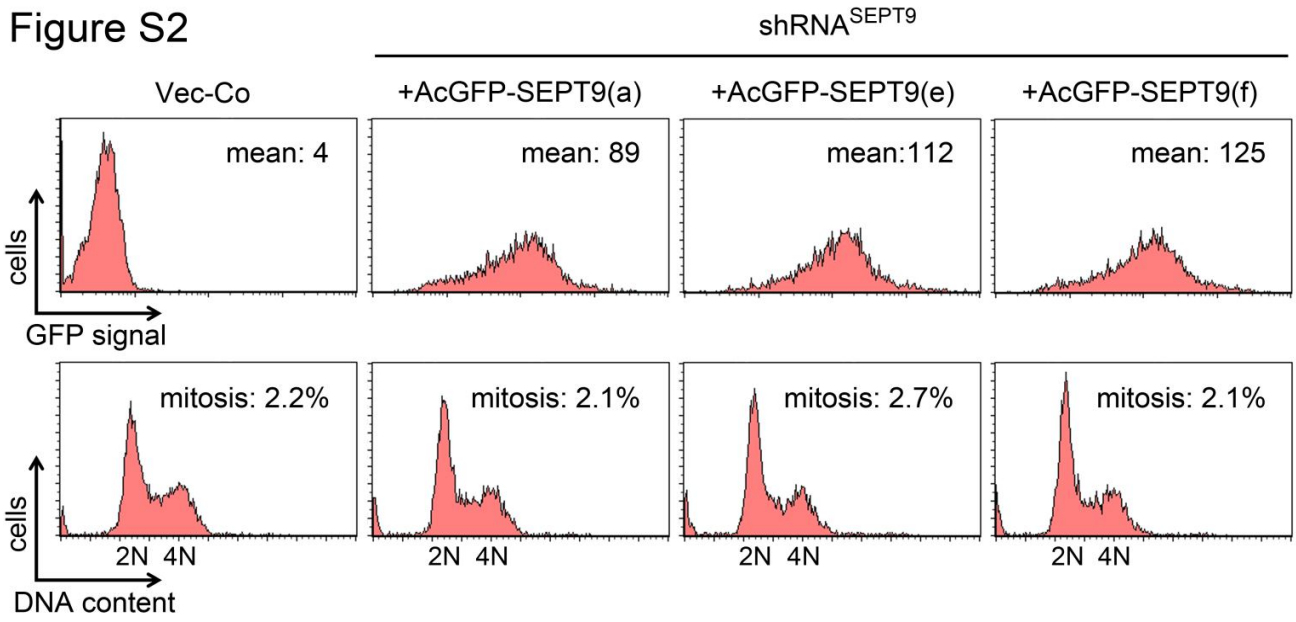

FIGURE S2: Fluorescence intensities of individual cells in which the endogenous SEPT9 isoforms are replaced with AcGFP-tagged versions of the indicated SEPT9 isoform.
Upper Panels: Cell lines described in Figure 5 were analyzed by flow cytometry. The distribution of background (Vector-Co) and AcGFP-fluorescence among live cells harboring shRNA^{SEPT9} and the indicated SEPT9 isoform reporter is shown. The mean fluorescence intensity of cells is indicated in each panel. More than 97% of all cells were included in the acquisition gate and 5000 cells were analyzed.
Lower Panels: Cell lines described in Figure 5 were stained with propidium iodide followed by analysis of DNA content by flow cytometry. The mitotic index of cells is indicated in each panel. The data shown in upper and lower panels were reproduced in three independent transfection experiments. Analysis by flow cytometry is described in (Holmfeldt *et al.*, 2003).

Interpretations:
The distribution of AcGFP-fluorescence intensity among individual cells in Figure S2 shows that AcGFP-SEPT9 expression varies within the cell population and that a significant fraction contains comparably low levels of the fluorescent reporter. Recall that these cells essentially lack endogenous SEPT9 (Figure 5B), which implies that the present results, combined with data in Figure S1A, predict a subpopulation of cells in which the ratio of octameric to hexameric heteromers is low. This subpopulation is identifiable by a comparably weak fluorescence (Figure 5C).

The DNA-profiles shown in Figure S1, lower panels, suggest that the present manipulations of SEPT9 isoform expression do not significantly interfere with cell growth. Moreover, we did not note any increase of the mitotic index (see inserts in Figure S2, lower panels). It is notable that depletion of the native septin heteromer pool by means of shRNA^{SEPT7} expression, or depletion of octamers by means of shRNA^{SEPT9} expression, does not cause a detectable mitotic phenotype in cell lines of hematopoietic origin, such as K562 and Jurkat cells (Sellin *et al.*, 2011a). This is contrast to adhesion-substrate dependent cell lines such as HeLa cells and embryonic mouse fibroblasts, but the reported defects during cell divisions are still relatively mild and only detectable in a subpopulation of cells (Estey *et al.*, 2010; Fuchtbauer *et al.*, 2011). There are presently no clues concerning cell type-specific differences with respect to the function of the septin system. Even so, it is still notable that deletion of septin genes in unicellular fungi like *Saccharomyces cerevisiae* and *Schizosaccharomyces pombe* results in different phenotypes and that the phenotype is subtle in the latter fungi (Oh and Bi, 2011).

SUPPLEMENTAL MATERIAL:

Primer pairs used for RT-PCR analysis SEPT9 transcript variant 1 to 7

Splice variant	Forward	Reverse	bp*
SEPT9_v1:	5′- GCCCAGGATTAGCGCCCTGG	5′- GACGCCTTGGGGGAGCGTTG	347
SEPT9_v2:	5′- GCTGCCCACCAGCCATCATGT	5′- GCCCTCTTGAGCCCGAACCG	400
SEPT9_v3:	5′- TGGTCTGCCGGACTCCTCGG	5′- GGGTGTCTCGACCTCCTCGACC	398
SEPT9_v4:	5′- GGAGGCTGCTCCAGTGTGCAT	5′- CGTAGCCGAAGTCCACCGGG	395
SEPT9_v5:	5′- TCTGCCCTGAGTGTGTGGGTCC	5′- GCGGGCCGAGGGTTCTGAGT	395
SEPT9_v6:	5′- GGAGAGGGGGCTGGGGCATAA	5′- ACGCCTTGGGGGAGCGTTG	390
SEPT9_v7:	5′- TCTGGCAGATCCCAGCGTCCA	5′- TCATGGCCTTCCGGCGCATCT	382

***** Length of PCR product

Construction of pMEP4 derivates directing regulatable expression of SEPT9 transcript variant 1, 5/6 and 7 (As indicated in Figure 1A, the cognate protein isoforms are termed SEPT9 isoform a, e and f according to NCBI Refseq)

A cDNA copy of sequence verified SEPT9 transcript variant 1 (accession NM_001113491.1, purchased from Origen, Cat. No. SC318940) was cloned as a *Not*I fragment into the corresponding site of the pMEP4 vector (termed pMEP-SEPT9(a)). The expressed native and AcGFP-fused SEPT9 isoforms were all made resistant to shRNA^{SEPT9} mediated suppression by introducing 4 silent mutations within the 19-nt shRNA-targeting sequence (CAC CAC ACA CTG TGA GTT T), which is located adjacent to the unique *Kpn*I site of SEPT9 cDNA. The silent mutations were introduced by PCR using pMEP-SEPT9(a) as a template and the following primer pair:

Forward primer containing 4 substitutions and covering the unique *Kpn*I site of SEPT9:
5'-GTGGGGTACCATCGAAGTTGAAAATACTACCCATTGTGAGTTTGC
Reverse primer located adjacent to the *Not*I site of the pMEP4 vector:
5'-CACTGCATTCTAGTTGTGG

The mutagenized PCR fragment was digested with *Kpn*I and *Not*I and inserted into the corresponding sites of pMEP4, which provided an intermediate derivative for construction of shRNA^{SEPT9} immune versions of SEPT9 isoforms (termed pMEP-SEPT9-*Kpn*I-sh616imm). To construct pMEP derivatives directing expression of shRNA^{SEPT9} immune SEPT9 isoforms, pMEP-SEPT9(a) was used as a PCR-template with a common reverse primer, which covers the unique *Kpn*I site of SEPT9 (5'-GGTGTTTTCAACTTCGATGGTACC), and forward primers that extend over the ATG initiation codon of SEPT9 isoform a, e and f. PCR fragments were digested with *Kpn*I and inserted into the corresponding site of pMEP-SEPT9-*Kpn*I-sh616imm, which regenerated the native open reading frames of SEPT9 isoform a, e and f.

Isoform-specific forward primers*:

*Kpn*I *Hind*III

SEPT9(a): 5'-ACTCGGTACCAAGCTT*GGAGGCACC***ATG**AAGAAGTC
SEPT9(e): 5'-ACTCGGTACCAAGCTT*TCAGCCCACCGGAGG***ATG**GAG
SEPT9(f): 5'-ACTCGGTACCAAGCTT*AGCTGCGTTGGCGAC***ATG**G

* Nucleotides corresponding to the 5' untranslated sequence preceding the **ATG** initiator codon of each isoform are italicized.

To construct SEPT9 isoform reporters with AcGFP fused to their N-terminus, a PCR generated fragment of AcGFP was inserted into the *Hind*III site introduced by the isoform-specific forward primers. The template and primers used to create the AcGFP-fragment with *Hind*III sites at both ends were as follows:

Template: pAcGFP1-N1 (Cat. No. 632469, Clontech Laboratories, Mountain View, CA).
5'-primer: 5'-GGACCCAAGCTTCTATTCACCATGGTGAGCAAGGGCGCCGAG
3'-primer: 5'-GGGTCCAAGCTTCTTGTACAGCTCATCCATGCC
The coding sequences of all PCR-generated fragments were confirmed by nucleotide sequence analysis.

REFERENCES

Estey, M.P., Di Ciano-Oliveira, C., Froese, C.D., Bejide, M.T., and Trimble, W.S. (2010). Distinct roles of septins in cytokinesis: SEPT9 mediates midbody abscission. J Cell Biol *191*, 741-749.

Fuchtbauer, A., Lassen, L.B., Jensen, A.B., Howard, J., Quiroga Ade, S., Warming, S., Sorensen, A.B., Pedersen, F.S., and Fuchtbauer, E.M. (2011). Septin9 is involved in septin filament formation and cellular stability. Biol Chem *392*, 769-777.

Holmfeldt, P., Brattsand, G., and Gullberg, M. (2003). Interphase and monoastral-mitotic phenotypes of overexpressed MAP4 are modulated by free tubulin concentrations. J Cell Sci *116*, 3701-3711.

Oh, Y., and Bi, E. (2011). Septin structure and function in yeast and beyond. Trends Cell Biol *21*, 141-148.

Sellin, M.E., Holmfeldt, P., Stenmark, S., and Gullberg, M. (2011a). Microtubules support a disk-like septin arrangement at the plasma membrane of mammalian cells. Mol Biol Cell *22*, 4588-4601.

Sellin, M.E., Sandblad, L., Stenmark, S., and Gullberg, M. (2011b). Deciphering the rules governing assembly order of mammalian septin complexes. Mol Biol Cell *22*, 3152-3164.

Wittig, I., Braun, H.P., and Schagger, H. (2006). Blue native PAGE. Nat Protoc *1*, 418-428.